Available online at www.sciencedirect.com
SCIENCE DIRECT®
Journal of Molecular Graphics and Modelling 24 (2005) 121–127
Journal of Molecular Graphics and Modelling
www.elsevier.com/locate/JMGM

Implementation of the bisection sampling method in path integral simulations

Dan Thomas Major *, Jiali Gao

Department of Chemistry, University of Minnesota, Minneapolis, MN 55455, USA

Available online 3 June 2005

Dedicated to Professor Ian Hillier for his contributions to the understanding of enzymatic reaction mechanisms.

Abstract

A bisection sampling method is implemented in the framework of a quantized classical path algorithm to include nuclear quantum effects in path integral simulations. The present study examines the convergence of these calculations on two model systems with respect to the number of beads used in the polymer chain and the number of configurations both in free-particle sampling and in classical configuration sampling. The results will be useful for future studies of kinetic isotope effects in enzymatic reactions.

Keywords: Bisection sampling method; Path integral simulation; Polymer

1. Introduction

Proton and hydride transfer reactions play an important role in many chemical and enzymatic reactions, and numerous studies of these processes in the gas phase, solution phase, and enzymes have been carried out. In particular, the significant role of quantum mechanical (QM) dynamical effects in enzyme catalysis has received considerable attention, evidenced by the unusual experimental kinetic isotope effects in several enzyme systems including the hydride transfer reaction in liver alcohol dehydrogenase and the proton transfer reaction in methylamine dehydrogenase [1–6]. Furthermore, a number of theoretical studies have shown that quantization of bound vibrational motions, especially the inclusion of zero point energy, can significantly reduce the free energies of activation of enzyme reactions [7–9]. Although methods that incorporate quantum mechanical dynamical effects in gas phase reactions have been well-established, enzymatic and condensed phase reactions require a method that can be used to average quantum effects over a myriad of conformations [10,11]. This is most easily accomplished by computing the potential of mean force (PMF) along a reaction coordinate using classical Monte Carlo or molecular dynamics simulations [12–14], and then, the effects of quantized molecular vibrations and quantum mechanical tunneling are incorporated into the rate calculation by a transmission coefficient [8,9,11,14–16]. Thus,

$$k^{\mathrm{qu}} = \gamma k^{\mathrm{TST}} \tag{1}$$

where k^{qu} is the quantum mechanical rate constant and k^{TST} is the classical transition state theory (TST) rate constant. In general, the transmission coefficient in Eq. (1) is a product of the deviation from equilibrium behavior, the classical dynamic recrossing factor, Γ, and the quantum mechanical correction, κ [16]. The latter is defined as

$$\kappa = \mathrm{e}^{-\beta(G^{\neq}_{\mathrm{qm}} - G^{\neq}_{\mathrm{TST}})} \tag{2}$$

where $\beta = 1/k_{\mathrm{B}}T$, k_{B} is Boltzmann's constant, T is the temperature, and $G^{\neq}_{\mathrm{qm}}$ and $G^{\neq}_{\mathrm{TST}}$ are the quantum and classical free energy of activation, respectively.

Previously, we have adopted this strategy by using a semiclassical theory that incorporates multidimensional tunneling contributions, and we have successfully applied this ensemble-averaged variational transition state theory (EA-VTST) to several enzymatic reactions with excellent

* Corresponding author.
E-mail address: major@chem.umn.edu (D.T. Major).

1093-3263/$ – see front matter © 2005 Elsevier Inc. All rights reserved.
doi:10.1016/j.jmgm.2005.04.002

agreement between the calculated and experimental kinetic isotope effects [17]. An alternative approach is to use the path integral formulation of quantum mechanics, in which the isomorphism between the discretized path integral (DPI) and a classical system allows one to evaluate quantum effects using classical simulation techniques [18–20]. Here, a quantum particle is represented by a ring of classical beads with their effective interaction described by a harmonic potential that has a force constant proportional to the number of classical particles in the chain, P [19]. At the limit of infinitely large P, the correspondence of the equilibrium properties of a quantum system and the isomorphic classical system is exact. The DPI approach is particularly suited for systems with a large number of degrees of freedom, such as condensed phase solute/solvent systems or macromolecular biomolecules.

In principle, the quantum mechanical free energy of activation, $G^{\neq}_{\mathrm{qm}}$, can be obtained directly by using centroid path integral molecular dynamics simulations [21–24]. However, it is more convenient to evaluate the free energy difference, $G^{\neq}_{\mathrm{qm}} - G^{\neq}_{\mathrm{TST}}$, in Eq. (2), by making a quantum correction to the classical mechanical (CM) potential of mean force evaluated from molecular dynamics simulations [15,25–27]. This correction can be enumerated either by Monte Carlo or molecular dynamics simulations over the classical trajectories. To this end, Sprik et al. [25] described a procedure to obtain properties by averaging quantum corrections over classical configurations, through free-particle path integral sampling by constraining the center of mass (centroid) of the beads within a small cubic volume.

$$\langle A \rangle = \langle \langle A \rangle_{\mathrm{K}}^{\mathrm{FP}} \rangle \tag{3}$$

In Eq. (3), the inner average $\langle A \rangle_{\mathrm{K}}^{\mathrm{FP}}$ represents the quantum average of property A by free-particle path integral over a fixed configuration K obtained from a separate, classical Monte Carlo simulation. The outer average is over these Monte Carlo configurations. This double averaging strategy was further exploited by Warshel and coworkers [15], who constrained the centroid position of the quantized particle to that of the corresponding classical coordinates [26–28]. This procedure, termed the quantized classical path (QCP), utilizes the trajectory obtained from classical mechanics simulations to obtain the QM correction by performing free-particle path integral averaging with the centroid constrained to the classical position. The QCP method is well suited to treat nuclear QM effects of large macromolecular systems, and has been applied to several enzymatic systems and has been compared to experimental and exact theoretical results with good agreement [15,26,29,30].

However, the convergence in PI implementations in general and in the QCP method in particular is not a trivial matter. Although a number of techniques for free-particle path integral sampling have been proposed [31], it appears that a direct sampling procedure was used in previous QCP applications to enzymatic reactions. A detailed description of the method was presented by Aqvist and coworkers who applied the QCP approach to the calculation of the kinetic isotope effect in the proton transfer reaction catalyzed by Glyoxalase I [29]. In this study, 20 beads were employed to describe the quantized particles, and 1, 5, and 10 Monte Carlo Metropolis steps were used to obtain the quantum correction for each classical configuration. In another calculation, a total of 20,000 free-particle configurations were used for 18 beads along the entire reaction coordinate for an enzymatic reaction [30]. However, other studies suggest that extensive path integral sampling is needed even for a dilute hard-sphere system [25], and it appears that a detailed study of the convergence behavior of the QCP method is desirable.

In this study, we report an implementation of the quantum correction algorithm, employing an efficient bisection method [31] coupled with the QCP approach to perform path integral sampling (BQCP), and present a detailed analysis of the convergence of the method for model systems.

2. Theoretical background

The canonical QM partition function of the system is written as an integral over the trace of the density matrix:

$$Q^{\mathrm{qu}} = \int \mathrm{d}\mathbf{x}\rho(\mathbf{x},\mathbf{x};\beta) \tag{4}$$

where $\beta = 1/k_{\mathrm{B}}T$, and the coordinate representation of the density operator is $\rho(\mathbf{x},\mathbf{x};\beta) \equiv \langle \mathbf{x}|\mathrm{e}^{-\beta H}|\mathbf{x}\rangle$, in which H is the Hamiltonian operator of the system. For convenience of presentation, we limit our discussion to one dimension. In the path integral formulation, the density operator is written as integrals over all possible paths of the particles in the system:

$$\rho(\mathbf{x},\mathbf{x};\beta) = \int_{\mathbf{x}(0)=\mathbf{x}(\beta\hbar)} \mathrm{D}\mathbf{x}(\tau)\mathrm{e}^{-1/\hbar S[\mathbf{x}(\tau)]} \tag{5}$$

where $\hbar = h/2\pi$, h is Planck's constant, and the integral

$$\int_{\mathbf{x}(0)=\mathbf{x}(\beta\hbar)} \mathrm{D}\mathbf{x}(\tau)[\cdots] \tag{6}$$

denotes integration over all paths beginning at $\mathbf{x}(0)$ and ending at $\mathbf{x}(\beta\hbar)$. In Eq. (5), the imaginary time action functional for the path $\mathbf{x}(\tau)$ is given as

$$S[\mathbf{x}(\tau)] = \int_0^{\beta\hbar} H[\mathbf{x}(\tau)]\,\mathrm{d}\tau = \int_0^{\beta\hbar} \left\{ \frac{m}{2}\dot{\mathbf{x}}(\tau)^2 + U[\mathbf{x}(\tau)] \right\} \mathrm{d}\tau \tag{7}$$

where $U[\mathbf{x}(\tau)]$ is the potential energy function.

If one defines the average or centroid position, $\bar{\mathbf{x}}$, of the path $\mathbf{x}(\tau)$:

$$\bar{\mathbf{x}} = \frac{1}{\beta\hbar}\int_0^{\beta\hbar} \mathrm{d}\tau \mathbf{x}(\tau) \tag{8}$$

the centroid density can be written as follows

$$\rho(\mathbf{x}_\mathrm{c};\beta) = \int_{\mathbf{x}(0)=\mathbf{x}(\beta\hbar)} \mathrm{D}\mathbf{x}(\tau)\delta(\mathbf{x}_\mathrm{c}-\bar{\mathbf{x}})\,\mathrm{e}^{-1/\hbar S[\mathbf{x}(\tau)]} \tag{9}$$

Then, the partition function can be defined in terms of the centroid density as

$$Q^\mathrm{qu} = \int \mathrm{d}\mathbf{x}_\mathrm{c}\rho(\mathbf{x}_\mathrm{c};\beta) \tag{10}$$

In the discrete path integral (DPI) form, each QM particle is described by a ring of P quasi-particles or beads, and the centroid QM partition function becomes

$$Q_P^\mathrm{qu} = \int \mathrm{d}\bar{\mathbf{x}}\left(\frac{1}{4\pi\Lambda^2}\right)^{P/2}\int \mathrm{d}x_1\cdots\int \mathrm{d}x_P\,\mathrm{e}^{-\beta V^\mathrm{qu}} \tag{11}$$

where the effective potential $V^\mathrm{qu}(x_1, \ldots, x_\mathrm{p})$ is given by

$$V^\mathrm{qu}(x_1,\ldots,x_\mathrm{p}) = \frac{1}{4\beta\Lambda^2}\sum_k^P (x_k - x_{k+1})^2 + \frac{1}{P}\sum_k^P U(x_k) \tag{12}$$

In Eqs. (11) and (12), Λ is the thermal de Broglie wavelength:

$$\Lambda = \left(\frac{\beta\hbar^2}{2mP}\right)^{1/2} \tag{13}$$

where m is the mass of the particle. Thus, each quasi-particle interacts via a harmonic spring with its two neighbors corresponding to a quantized kinetic energy. Each of the quasi-particles is subject only to a fraction, $1/P$, of the full classical potential, U. The discrete paths are circular with $x_{P+1} = x_1$. The exact QM partition function is obtained in the limit:

$$Q^\mathrm{qu} = \lim_{P\to\infty} Q_P^\mathrm{qu} \tag{14}$$

In the QCP approach [26], one defines a reference classical partition function as follows:

$$Q_P^\mathrm{cl} = \int \mathrm{d}\bar{\mathbf{x}}\left(\frac{1}{4\pi\Lambda^2}\right)^{P/2}\int \mathrm{d}x_1\cdots\int \mathrm{d}x_P\,\mathrm{e}^{-\beta U^\mathrm{sc}} \tag{15}$$

where the semi-classical potential is defined as

$$U^\mathrm{sc} = \frac{1}{4\beta\Lambda^2}\sum_k^P (x_k - x_{k+1})^2 + \frac{1}{P}\sum_k^P U(\bar{x}) \tag{16}$$

In Eq. (16), the quantized kinetic energy part is retained, but the potential energy is classical since it is localized at the centroid position, $\bar{x}$. Warshel et al. [15,26] showed that the QM correction to classical free energy along a reaction path defined by the centroid position may be written as follows:

$$G_\mathrm{qm}^{\neq} - G_\mathrm{TST}^{\neq} = -\frac{1}{\beta}\ln\frac{Q_P^\mathrm{qu}}{Q_P^\mathrm{cl}} = -\frac{1}{\beta}\ln\left\langle\left\langle \mathrm{e}^{-(\beta/P)\sum_k^P \Delta U_k}\right\rangle_{\mathrm{FP},\bar{x}}\right\rangle_U \tag{17}$$

where $\Delta U_k = U(x_k) - U(\bar{x})$. Here, the outer average $\langle\cdots\rangle_U$ is obtained according to the distribution generated by propagating classical molecular dynamics or Monte Carlo simulations using the potential $U(\bar{x})$. The inner average $\langle\cdots\rangle_{\mathrm{FP},\bar{x}}$ is over the free-particle distribution, in the absence of any external potential:

$$\left\langle \mathrm{e}^{-(\beta/P)\sum_k^P \Delta U(x_k)}\right\rangle = \frac{\int \mathrm{e}^{-(\beta/P)\sum_k^P \Delta U(x_k)}\,\mathrm{e}^{-(1/4\beta\Lambda^2)\sum_k^P (x_k - x_{k+1})^2}\,\mathrm{d}x_1\cdots\mathrm{d}x_P}{\int \mathrm{e}^{-(1/4\beta\Lambda^2)\sum_k^P (x_k - x_{k+1})^2}\,\mathrm{d}x_1\cdots\mathrm{d}x_P} \tag{18}$$

In Eq. (18), the integration of beads is constrained at the centroid position $\bar{x}$. The advantage of this formulation is that one can sample the free-particle (FP) distribution (i.e. the quasi-particle polymer rings) separately at each CM configuration (i.e. centroid position) and then average over all CM configurations obtained from molecular dynamics simulations.

3. Methods

3.1. Convergence

Although Eqs. (17) and (18) provide a very appealing framework for obtaining quantum averages by carrying out classical simulations on a classical potential $U(\bar{x})$ rather than on the quantum potential $V^\mathrm{qu}(x_1, \ldots, x_\mathrm{p})$ of Eq. (12) itself, a main practical problem is that only a tiny fraction of the free-particle configurations may actually be favorable in the external potential $U(\bar{x})$ and contribute significantly to the average of Eq. (18). The vast majority of the free-particle configurations make little contribution to the integral of Eq. (18). Thus, unless an efficient free-particle sampling procedure is used, it would be very difficult to achieve convergence using Eq. (18), with respect to either the length of the free-particle trajectory or the number of path integral beads.

In QCP calculations, it is possible that one could find a subset of the polymer bead configurations that carry the greatest weight, and ignore the multiple configurations that contribute negligibly to the path integral average. However, for a given potential energy surface, these polymer ring configurations are generally not known. Therefore, it is necessary to comprehensively sample the free-particle distribution. Moreover, to assure accurate results from PI calculations, it is necessary to increase the number of beads

until the desired property is converged. This introduces a problem since the spring connecting the polymer beads becomes increasingly stiff as the number of beads increases, which makes it even more difficult to sample. In fact, the equilibration time of the slowest mode in the ring polymer scales as $(P/\pi)^2$ where P is the number of beads [31]. Thus, standard Metropolis Monte Carlo and molecular dynamics simulations are not the optimal choice as a free-particle sampling algorithm, which has been pointed out previously [32].

A number of techniques have been suggested for path integral sampling in Monte Carlo or molecular dynamics simulations [31]. We found that the bisection scheme introduced by Ceperley and coworkers is most effective in our implementation. This approach takes advantage of the fact that the non-interacting density matrix yields a Gaussian equilibrium distribution of known mean and width:

$$\rho(x_i, x_m; \beta/P) = \left(\frac{1}{4\pi\sigma}\right)^{1/2} \mathrm{e}^{(x_i - x_m)^2/2\sigma} \tag{19}$$

where the variant of the Gaussian is the square of the de Broglie wavelength $\sigma = \Lambda^2$, and

$$x_m = \frac{x_{i-1} + x_{i+1}}{2} \tag{20}$$

Therefore, the free-particle distribution can be sampled exactly with 100% acceptance in a Monte Carlo simulation according to the Gaussian distribution (Eq. (19)). A straightforward application of this approach is to move one bead in each Monte Carlo step, but an even more efficient algorithm is to make multiple moves without reducing the Monte Carlo step size.

Sprik et al. proposed a staging technique in Monte Carlo path integral simulations [25]. Here, we implement the bisecting method proposed by Ceperley [31], which is a combination of multilevel Monte Carlo [33] and the Levy construction for sampling a free-particle path [34]. The bisection method takes advantage of the fact that the density matrix at a given temperature may be written as the integral of two density matrices at a higher temperature [31]. Thus, one can accurately sample the free-particle distribution at a higher temperature and more effectively explore the configurational space.

Specifically, for each Monte Carlo step, we select at random a sequence of $N-1$ consecutive beads along the ring polymer, where $N = 2^l$ and l is the level of bisection. Enclosing the bead sequence are two fixed endpoints located at r_i and r_{i+N}. In principle, the two endpoints could be the same bead, when the entire polymer ring is sampled at each MC step, which will generate entirely uncorrelated MC steps. At the coarsest level of bisection, $k = l$, the position of the bead in the midpoint of the sequence is first sampled, which is placed at the geometrical center of the two end points and randomly displaced according the Gaussian distribution of width $2^{l-1}\sigma$, $r_{i+N/2} = (r_i + r_{i+N})/2 + \xi$, where ξ is the random displacement vector. Having sampled the $r_{i+N/2}$ point, we bisect the two new intervals $(r_i, r_{i+N/2})$ and $(r_{i+N/2}, r_{i+N})$ at the next bisection level $k = l - 1$ with the distribution width $2^{l-2}\sigma$, to sample points at $r_{i+N/4}$ and $r_{i+3N/4}$. This bisecting procedure continues recursively until level $k = 1$, where all $N-1$ beads have been sampled. As in the single bead sampling, the acceptance ratio for such a Monte Carlo move will be 100% since the new positions are drawn from the accurate free-particle distribution [31]. After each MC step the ring polymers are centered around the centroid position to enforce the centroid constraint. In our implementation, the Box–Muller transformation is used to generate the random displacements with a Gaussian distribution [35].

3.2. Model systems

We choose two model systems to test the bisection sampling method in QCP calculations. The first system is a Morse potential:

$$V(x) = D_\mathrm{e}[1 - \mathrm{e}^{-\alpha(x-x_0)}]^2 \tag{21}$$

where $D_\mathrm{e} = 136.3$ kcal/mol, $\alpha = 2.2112$ Å^{-2}, and $x_0 = 0.9166$ Å. The values were chosen to resemble those of the HF molecule [36]. The Morse oscillator was treated as a one-dimensional problem in Cartesian coordinates. The second model is the symmetric Eckart potential with the following parameters:

$$V(x) = V_\mathrm{max}\,\mathrm{sech}^2\left(\frac{\pi x}{l}\right) \tag{22}$$

where $V_\mathrm{max} = 5.7307$ kcal/mol and $l = 1.0967$ [37].

4. Results

4.1. The Morse potential

We first test the convergence of the free-particle sampling procedure with respect to the number of beads in the polymer ring, the extent of free-particle sampling, and the number of classical Monte Carlo steps. Table 1 shows the QM free energy correction over classical Monte Carlo configurations for a single particle in a Morse potential. The results are obtained by the free-particle bisection sampling method over different number of beads in the polymer ring and different number of classical configurations. Initially, we performed a simulation of free particles for a single classical configuration located at the minimum of the Morse potential. The free-particle sampling was performed over 1000 configurations. It is clear from the third column of Table 1 that 64 beads or more are required to reach a converged result, although the average value obtained using 32 beads is within statistical uncertainty. Below 32 beads, the QM corrections are consistently underestimated. This is consistent with previous findings [26]. In Table 1, the

Table 1
Average quantum mechanical correction (kcal/mol) from BQCP simulations for the Morse potential vibrational partition function (given as $G^{\neq}_{qm} - G^{\neq}_{TST} = -RT \ln(Q_{qm}/Q_{cl})$) at $T = 300$ K

P[a]	k[b]	$G^{\neq}_{qm} - G^{\neq}_{TST}$ (Cl Monte Carlo/PI steps)[c]							Exact[d]
		1/1000[e]	10/1000	100/1000	1000/10	1000/100	1000/1000	10000/10000	
8	3	3.18 ± 0.15	3.48 ± 0.25	3.03 ± 0.26	3.01 ± 1.35	3.06 ± 0.39	3.10 ± 0.24	3.08 ± 0.22	3.98
16	4	3.80 ± 0.12	3.70 ± 0.20	3.75 ± 0.35	3.63 ± 1.25	3.64 ± 0.50	3.65 ± 0.37	3.66 ± 0.30	
24	4	3.94 ± 0.11	3.87 ± 0.31	3.71 ± 0.40	3.95 ± 1.29	3.87 ± 0.49	3.80 ± 0.35	3.82 ± 0.33	
32	5	3.98 ± 0.11	3.91 ± 0.25	3.82 ± 0.36	3.87 ± 1.18	3.84 ± 0.47	3.91 ± 0.35	3.88 ± 0.34	
64	6	4.09 ± 0.09	4.14 ± 0.41	3.85 ± 0.38	3.91 ± 1.19	3.96 ± 0.50	3.94 ± 0.36	3.97 ± 0.35	
128	7	4.02 ± 0.08	4.22 ± 0.20	3.98 ± 0.29	3.94 ± 1.34	3.95 ± 0.46	3.99 ± 0.36	3.96 ± 0.37	
256	8	4.09 ± 0.10	4.04 ± 0.16	4.09 ± 0.30	4.06 ± 1.24	3.98 ± 0.50	3.98 ± 0.38	3.97 ± 0.36	

[a] Number of beads used to calculate PI.
[b] The number of beads moved at each MC step was defined as $2^k - 1$.
[c] PI averaged over multiple classical configuration. Cl = classical MC steps for Morse oscillator. PI = path integral steps. Standard deviation is for classical MC steps, with the exception of the first column.
[d] Calculated from exact classical and QM partition functions.
[e] Classical configuration corresponds to bottom of the Morse potential well. Standard deviation is for 10 independent simulations.

standard deviation is gradually decreased by extending the number of free-particle sampling steps (up to 10,000 Monte Carlo steps in the present test for each classical configuration) as the quantum correction approaches convergence for a given number of beads used in the path integral sampling. The bisection sampling method yields converged results with increasing number of beads, in contrast to calculations by randomly sampling free-particle configurations (using Metropolis Monte Carlo), where Eq. (17) converge extremely slowly even after 100,000 free-particle configurations. In the present implementation, we find that the sampling efficiency is independent of the number of beads used, despite the increased complexity with greater polymer ring size. This is due to the bisection algorithm, which samples the free-particle distribution exactly.

Table 1 shows that to obtain converged results using Eq. (17), both the quantum correction at each classical configuration and the overall free energy difference between the quantum and classical system must be obtained. The former is concerned with free-particle sampling at a given classical configuration, which defines the free-particle centroid position. On the other hand, the latter convergence is over the Boltzmann weight of the classical potential energy surface. In this test case of a simple Morse oscillator, a minimum of 100 free-particle configurations are required for a given classical (centroid) position. Indeed, the results obtained by using 10 free-particle sampling steps have relatively greater errors compared to the best converged result by using 10,000 free-particle configurations per centroid position. The use of 1000 path-integral steps only slightly improves the convergence relative to 100 free-particle configurations.

Table 1 also shows that the accuracy of the QM correction is critically dependent on the number of classical Monte Carlo configurations used in the outer average of Eq. (17). This is because the average QM correction of Eq. (18) at each classical configuration has large variations depending on the centroid position. Here, the average obtained over 100 classical configurations yield marginally converged values, while results do not show appreciable changes beyond 1000 classical configurations for all bead numbers used in the path integral sampling. Clearly, the rate of convergence of the final result is highly system dependent, and it is necessary to test the number of classical and free-particle configurations needed to achieve converged results for each system.

It is interesting to note that the converged result for the quantum correction to the classical free energy (partition function) of the Morse oscillator is in excellent agreement with the exact value, even with a moderate number of beads.

4.2. The symmetric Eckart barrier

The results for the symmetric Eckart barrier in Table 2 are in reasonable agreement with the exact values obtained by Shavitt [38]. Similar results were also obtained by Hwang and Warshel, although the computational details were not given except that 64 beads were used in their calculation [26]. The deviation of the present BQCP simulation from the exact values is likely due to a combination of factors including the centroid approximation near the top of the

Table 2
Computed quantum mechanical correction factor to the classical transition state theory rate constant for the Eckart potential of a hydrogen atom

T (K)	κ^{BQCP} [a]	κ^{exact} [b]
500	1.43	1.53
400	1.75	1.92
350	2.09	2.23
300	2.73	3.15
250	4.46	5.31
200	11.52	14.97
100	130.409	179.760

[a] $\kappa^{BQCP} = k^{qu}/k^{cl}$. The PI calculation used 32 beads and 10,000 MC steps.
[b] The exact QM correction factor was calculated as described by Shavitt [38].

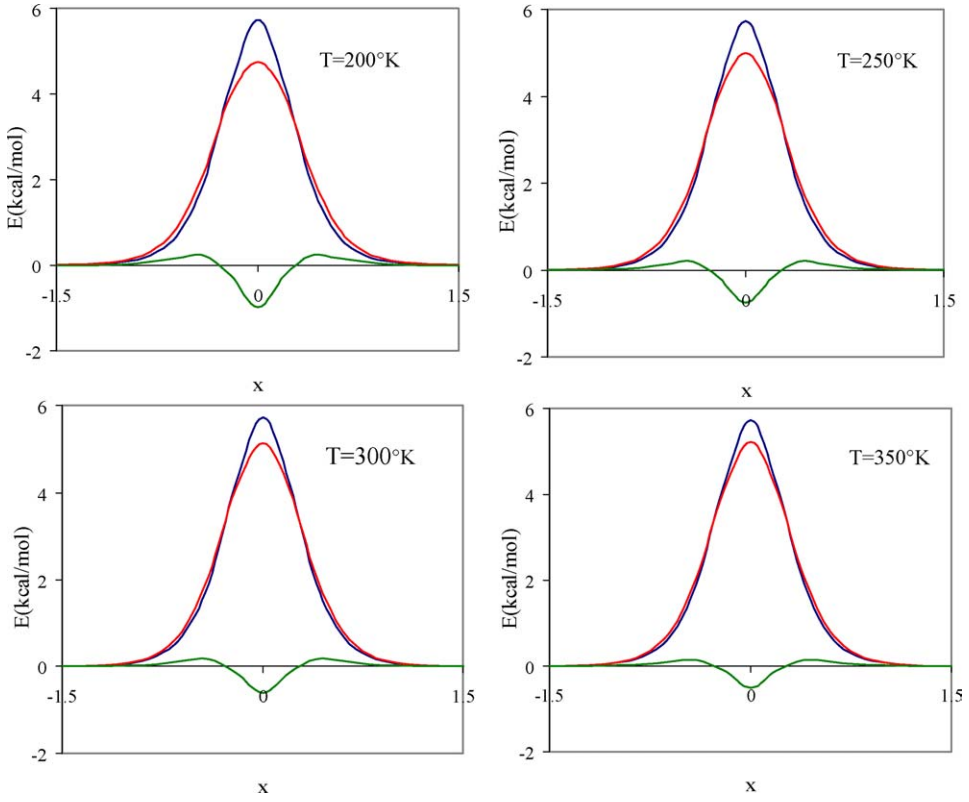

Fig. 1. Computed quantum (red) and classical (blue) potentials of mean force and quantum corrections (green) for a proton transfer over an Eckart potential as a function of the centroid position at different temperatures.

barrier, dynamical QM effects, and a finite number of beads used in the sampling. At low temperature the error becomes increasingly larger due to greater QM effects. At 300 K, the error is 13% corresponding to an underestimate of the QM correction by 0.24 kcal/mol. Although results listed in Table 2 were obtained with 32 beads in path integral sampling, we have also tested the convergence by using 256 beads at 300 K, which yielded results within 5% of the value for the 32-bead system.

In studies of enzymatic reactions, an important quantity that can be compared with experiment is kinetic isotope effects (KIEs), which provide a direct probe of the reaction mechanism. Previous studies have shown that it is essential to include quantum nuclear effects in enzyme kinetic modeling and KIE calculations. In Table 3, we compare the exact [38] and computed KIE from the present BQCP sampling for a model H/D transfer over the Eckart potential. The quantum correction factors for the hydrogen and deuterium transfer reactions are computed independently along the ''reaction coordinate'', x, which are depicted in Fig. 1 at four different temperatures. Clearly, the analysis accounts for the quantum effects. From Table 3, it is evident that the errors in the computed KIE are reduced relative to that of the transmission coefficient (Table 2). At 300 K, the KIE is underestimated by 0.14, which translates to an error of 8% in comparison to that from Ref. [38]. This error range is comparable to deviations in computed KIE from other theoretical methods [11].

Table 3
Computed kinetic isotope effects for the hydrogen and deuterium transfer over the Eckart potential at various temperatures

T (K)	$\kappa^{H}/\kappa^{D,BQCP}$ [a]	$\kappa^{H}/\kappa^{D,exact}$ [b]
500	1.19	1.23
400	1.31	1.37
350	1.43	1.51
300	1.62	1.76
250	2.08	2.28
200	3.33	3.84
100	156.48	106.03

[a] $\kappa^{BQCP} = k^{qu}/k^{cl}$. The PI calculation used 32 beads and 10,000 MC steps.
[b] The exact QM correction factor was calculated as described by Shavitt [38].

5. Conclusions

The quantized classical path (QCP) method developed by Hwang and Warshel provides a practical computational framework for estimating nuclear QM effects in condensed phase reactions. However, the convergence of the method has been difficult to achieve in our hands. Here, the QCP method was combined with the bisection algorithm (BQCP) to sample the free-particle distribution. A detailed study was performed to quantify the convergence and accuracy of the

method. This is a crucial step in the implementation of the QCP method into macromolecular simulation platforms. The current study showed that it is necessary to sample the quantized path as well as averaging over classical configurations. The use of 32 beads gives fairly converged values, while the use of 16 beads introduces considerably greater uncertainty in the results.

Acknowledgements

The work is partially supported by the National Institutes of Health and by the Army High-Performance Computing Research Center (AHPCRC) under the auspices of the Department of the Army, Army Research Laboratory under DAAD19-01-2-0014. Dan T. Major thanks the Fulbright Foundation for financial support. We thank Prof. D. Ceperley for helpful discussions.

References

[1] P.F. Faulder, G. Tresadern, K.K. Chohan, N.S. Scrutton, M.J. Sutcliffe, I.H. Hillier, N.A. Burton, J. Am. Chem. Soc. 123 (2001) 8604.
[2] Y. Cha, C.J. Murray, J.P. Klinman, Science 243 (1989) 1325.
[3] A. Kohen, J.P. Klinman, Chem. Biol. 6 (1999) 191.
[4] H.B. Brooks, L.H. Jones, V.L. Davidson, Biochemistry 32 (1993) 2725.
[5] J. Basran, M.J. Sutcliffe, N.S. Scrutton, Biochemistry 38 (1999) 3218.
[6] J. Basran, S. Patel, M.J. Sutcliffe, N.S. Scrutton, J. Biol. Chem. 276 (2001) 6234.
[7] C. Alhambra, J.C. Corchado, M.L. Sánchez, J. Gao, D.G. Truhlar, J. Am. Chem. Soc. 122 (2000) 8197.
[8] M. Garcia-Viloca, C. Alhambra, D.G. Truhlar, J. Gao, J. Chem. Phys. 114 (2001) 9953.
[9] S.R. Billeter, S.P. Webb, T. Iordanov, P.K. Agarwal, S. Hammes-Schiffer, J. Chem. Phys. 114 (2001) 6925.
[10] P.L. Fast, J.C. Corchado, D.G. Truhlar, J. Chem. Phys. 109 (1998) 6237.
[11] J. Gao, D.G. Truhlar, Ann. Rev. Phys. Chem. 53 (2002) 467.
[12] W.P. Keirstad, K.R. Wilson, J.T. Hynes, J. Chem. Phys. 95 (1991) 5256.
[13] M.J. Field, in: W.F. van Gunsteren, P.K. Weiner, A.J. Wilkinson (Eds.), Computer Simulation of Biomolecular Systems, vol. 2, ESCOM, Leiden, 1993, p. 82.
[14] M. Vieth, J.D. Hirst, C.L. Brooks III, J. Comput. Aided Mol. Des. 12 (1998) 563.
[15] J.-K. Hwang, Z.T. Chu, A. Yadav, A. Warshel, J. Phys. Chem. 95 (1991) 8445.
[16] M. Garcia-Viloca, J. Gao, M. Karplus, D.G. Truhlar, Science 303 (2004) 186.
[17] C. Alhambra, J. Corchado, M.L. Sánchez, M. Garcia-Viloca, J. Gao, D.G. Truhlar, J. Phys. Chem. B 105 (2001) 11326.
[18] (a) R.P. Feynman, A.R. Hibbs, Quantum Mechanics and Path Integrals, McGraw-Hill, New York, 1965;
(b) R.P. Feynman, Statistical Mechanics, Addison-Wesley, Reading, MA, 1972.
[19] (a) D. Chandler, P.G. Wolynes, J. Chem. Phys. 74 (1981) 7;
(b) G.A. Voth, D. Chandler, W.H. Miller, J. Chem. Phys. 91 (1989) 7749.
[20] B.J. Berne, Annu. Rev. Phys. Chem. 37 (1986) 401.
[21] G.A. Voth, J. Phys. Chem. 97 (1993) 8365.
[22] N. Chakrabarti, T. Carrington Jr., B. Roux, Chem. Phys. Lett. 293 (1998) 209.
[23] D. Marx, M.E. Tuckerman, G.J. Martyna, Comput. Phys. Comm. 118 (1999) 166.
[24] S.L. Mielke, D.G. Truhlar, Chem. Phys. Lett. 378 (2003) 317.
[25] M. Sprik, M.L. Klein, D. Chandler, Phys. Rev. B 31 (1985) 4234.
[26] J.-K. Hwang, A. Warshel, J. Phys. Chem. 97 (1993) 10053.
[27] J.-K. Hwang, A. Warshel, J. Am. Chem. Soc. 118 (1996) 11745.
[28] M.J. Gillan, J. Phys. C: Solid State Phys. 20 (1987) 3621.
[29] I. Feierberg, V. Luzhkov, J. Aqvist, J. Biol. Chem. 275 (2000) 22657.
[30] M.H.M. Olsson, P.E.M. Siegbahn, A. Warshel, J. Am. Chem. Soc. 126 (2004) 2820.
[31] D.M. Ceperley, Rev. Mod. Phys. 67 (1995) 279.
[32] E.L. Pollock, D.M. Ceperley, Phys. Rev. B 30 (1984) 2555.
[33] D.M. Ceperley, E.L. Pollock, Phys. Rev. Lett. 56 (1986) 351.
[34] P. Levy, Compos. Math. 7 (1939) 283.
[35] W.H. Press, B.P. Flannery, S.A. Teukolsky, W.T. Vetterling, Numerical Recipes: The Art of Scientific Computing, PN Cambridge University Press, USA, pp. 202–203.
[36] S.V. Khristenko, A.I. Maslov, V.P. Shevelko, in: I.I. Sobel'man (Ed.), Molecules and Their Spectroscopic Properties, Springer, Berlin, 1998.
[37] H.S. Johnston, Gas Phase Reaction Rate Theory, Ronald, New York, 1966, pp. 40–47.
[38] I. Shavitt, J. Chem. Phys. 31 (1959) 1359.